Transient growth associated with secondary vortices in ground/vortex interactions

Thomas A Stuart, Xuerui Mao* and Lian Gan

School of Engineering and Computer Science, Durham University, Durham, County Durham, DH1 3LE, UK

The interaction of an isolated trailing vortex and the ground is investigated. An unsteady unperturbed flow is firstly calculated through a two-dimensional direct numerical simulation and then used as base flow for linear transient growth studies. The transient growth increases with Reynolds number and maximises at streamwise wavenumber $3 \sim 5$ over the parameters considered. The most energetic initial perturbation is found to be located aside of the main vortex and convected by the base flow to the ground to interact with the separating boundary layer and the secondary vortex. Finally the calculated perturbation is used to perturb the base flow in three-dimensional direct numerical simulations. It is observed that the secondary vortex and the rebound motion of the main vortex are both significantly suppressed. This observation indicates that the secondary structures are sensitive to external noise and the widely reported secondary vortex and its induced rebound motion of the main vortex in two-dimensional DNS would not appear or become much weaker in real conditions.

Nomenclature

$\boldsymbol{u}$	velocity
$\boldsymbol{U}$	base velocity
$\boldsymbol{u}'$	perturbation velocity
$\hat{\boldsymbol{u}}$	Fourier decomposed velocity
p	pressure
P	base pressure
p'	perturbation pressure
Re	Reynolds number

*maoxuerui@sina.com

Ω computational domain

k spanwise wavenumber

T time interval for transient growth

G transient energy growth

q vortex swirl strength

R vortex radius

$\mathcal{P}$ polynomial order in the spectral element method

Subscript

x, y, z components in spanwise, vertical and streamwise directions, respectively

k Fourier modes with wavenumber k

I. Introduction

During takeoff, approach or landing, a pair of vortices are shed from the wing tips of an aircraft in ground proximity. It is well known that this vortex pair will descend towards the ground due to the downwash effect.[1] Once significantly close to the ground, the two vortices move apart from one another on a hyperbolic trajectory.[2] Whilst moving apart the vortices ascend away from the runway in a rebound motion.[3] This outward-rebound effect is induced by the secondary vortices stemming from the separated boundary layer on the ground.[4] Without sufficiently strong crosswinds this vortical system may not leave the flight corridor vertically or laterally and will decay slowly above the runway. Due to their strong coherent structures, these vortices generate rolling moments and impose a potential risk to the queuing aircraft.[5] Moreover, the possibility of the pilot to counteract the imposed rolling moment is restricted due to the low height of the aircraft above ground.[6] In this way, the trailing vortices impose constraints on the airport operation and aircraft design. Therefore an accurate prediction of the vortex/ground interaction is crucial for a wake-vortex advisory system so as to enhance the airport capacity.[7] This vortex/ground interaction also exists in flow around the front wing of a racing car, which operates within strong ground effect to generate downforce and improve the vehicle's performance.[8,9]

Previous studies of vortex/ground interactions have been concentrated on the dynamics of the secondary vortex, which is responsible for the rebound motion of the main vortex. Three-dimensional (3D) wavy features of the secondary vortex have been observed in experiments[4,10] and numerical simulations,[3] and asymmetric secondary vortices shed from the tip of aircraft have been recorded in airport measurements.[6] Most recently, it was observed that in two-dimensional (2D) simulations, the vortices are stronger and the paths are higher than in 3D simulations when the vortex is originally perturbed.[11] All these observations

indicate that the secondary vortex is sensitive to external perturbations and suggest a 3D instability. However stability and transient growth studies of vortex flow have been focused on an isolated vortex or a vortex pair while relatively less efforts have been devoted to the ground/vortex interaction. In this work, a simplified model consisting of an isolated Batchelor vortex and a ground boundary will be adopted to investigate the role of infinitesimal perturbations in the vortex/ground interaction. In this model, the unperturbed flow is homogeneous in the streamwise direction and therefore supports a BiGlobal analysis through decomposing the perturbation as Fourier modes with various streamwise wavenumbers. Such a BiGlobal analysis has been applied to study hydrodynamic stabilities of a vortex/pipe flow, where the unperturbed base flow exhibits a slow decay and can be frozen as steady.[12] However, in the present case, the vortex system featuring boundary layer separations and secondary vortex generations is highly unstable. Therefore non-normality or a transient energy growth analysis, which accommodates an unstable base flow, becomes an ideal tool to illustrate the linear dynamics of perturbations.

The linearly optimal initial perturbations will be further studied through direct numerical simulations (DNS). It will be clarified that the reduction of vortex strength and the rebound motion is owing to the suppression effects of transiently growing perturbations on the secondary vortex; and that the coherent vortex structures widely predicted in 2D simulations[13,14] cannot be persisted in real 3D developments.

II. Methodology

Start from the incompressible Navier-Stokes (NS) equations,

$$\partial_t \boldsymbol{u} = -(\boldsymbol{u}\cdot\boldsymbol{\nabla})\boldsymbol{u} - \boldsymbol{\nabla} p + Re^{-1}\boldsymbol{\nabla}^2\boldsymbol{u}, \quad \text{with} \quad \boldsymbol{\nabla}\cdot\boldsymbol{u} = 0,$$

where $\boldsymbol{u}$ and p are velocity and pressure, respectively. Re denotes the Reynolds number based on the maximum streamwise velocity of the vortex model and the initial distance between the vortex centre and the ground. The flow field can be decomposed into the summation of an unperturbed base flow and a perturbed flow as $(\boldsymbol{u}, p) = (\boldsymbol{U}, P) + (\boldsymbol{u'}, p')$. When the magnitude of the perturbation velocity is significantly smaller than that of the unperturbed flow, the perturbation can be governed by the linearised NS equations,

$$\partial_t \boldsymbol{u'} = -(\boldsymbol{U}\cdot\boldsymbol{\nabla})\boldsymbol{u'} - (\boldsymbol{u'}\cdot\boldsymbol{\nabla})\boldsymbol{U} - \boldsymbol{\nabla} p' + Re^{-1}\boldsymbol{\nabla}^2\boldsymbol{u'}, \quad \text{with} \quad \boldsymbol{\nabla}\cdot\boldsymbol{u'} = 0.$$

In this work, a Cartesian coordinate is adopted, with x, y and z denoting spanwise, vertical and streamwise directions respectively. The unperturbed base flow will be modelled as the Batchelor vortex, which is

homogeneous in the streamwise direction. Therefore the perturbation can be further decomposed as

$$\boldsymbol{u}'(x,y,z,t) = \sum_{k=0}^{\infty} \hat{\boldsymbol{u}}_k(x,y,t)\mathrm{e}^{\mathrm{i}kz}$$

where $\hat{\boldsymbol{u}}_k$ denotes the Fourier decomposed perturbation with streamwise wavenumber k. Owing to the linearisation of the governing equations, dynamics of modes with different wavenumbers are decoupled and can be calculated individually. In the following, the term perturbation will be referred to the Fourier decomposed mode and the subscript wavenumber will be omitted for clarity. In transient energy growth, the most energetic (optimal) initial perturbation over a given time horizont T at a prescribed streamwise wavenumber k is defined as the perturbation that maximises the ratio of the final energy and initial energy,

$$G = \max_{\hat{\boldsymbol{u}}(x,y,0)} \frac{E(T)}{E(0)} \qquad \text{where} \qquad E(t) = \int_{\Omega} \hat{\boldsymbol{u}}(x,y,t) \cdot \hat{\boldsymbol{u}}(x,y,t)\mathrm{d}V$$

denotes the kinetic energy of perturbations integrated over the computational domain Ω. This optimal perturbation and the corresponding value of G can be calculated by applying an Arnoldi method to a Krylov sequence built by iteratively integrating the linearised NS equations and the adjoint, or by optimising a Lagrangian functional,[15,16] both of which are well established methods and are not elaborated here.

III. Convergence and discretisation

The aircraft wake flow contains a pair of counter-rotating vortices shed from the wing tips. The interaction of the two vortices has been well studied.[4,17,18] In this work, a single vortex, modelled as the Batchelor vortex, is adopted to isolate the effect of ground/vortex interactions on the wake flow development. The velocity components of this vortex, normalised by the streamwise velocity at the vortex centre, are

$$\begin{aligned} U_x &= -\frac{qR(y-1)}{r^2}[1-\exp(-r^2/R^2)], \\ U_y &= \frac{qRx}{r^2}[1-\exp(-r^2/R^2)], \\ U_z &= \exp(-r^2/R^2), \end{aligned}$$

where $r = [x^2 + (y-1)^2]^{1/2}$, q denotes the swirl strength and R represents the initial core radius of the vortex. The vortex is initially centred at $(x, y) = (0, 1)$. A spectral element method is used to discretize the governing equations, e.g. the NS equations, linearised NS equations and the adjoint. A decomposition of the domain into 3, 638 spectral elements, with over 2000 elements located in the rectangular box accommodating the trajectory of the vortex, is shown in figure $1(a)$. The computational domain spans from -50 to 50 and 0

to 50 in spanwise and vertical directions, respectively, and the ground is located at $y = 0$. A zero Dirichlet velocity boundary condition is applied to all the boundaries. A preliminary study showed that the optimal perturbations develop around the main vortex and the secondary vortex. Therefore the resolution around the trajectory of the vortex is refined, as can be seen in figure 1(b). In each element, a spectral method is

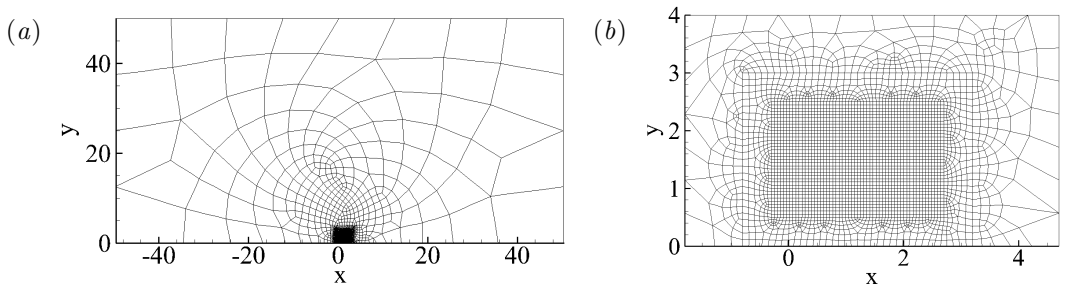

Figure 1. Computational grid for (a) the full domain and (b) subdomain surrounding the trajectory of the vortex.

used to further decompose the element to a $(\mathcal{P}+1)\times(\mathcal{P}+1)$ grid, where $\mathcal{P}$ represents a polynomial order and can be used to refine resolution in convergence tests.[19] Dependence of the maximum energy growth G with respect to $\mathcal{P}$ at $k = 1$, $Re = 3000$, $q = 0.8$, $R = 0.1$ and $T = 50$ is illustrated in table 1. It is seen that G has converged to three significant figures at $\mathcal{P} = 4$. Therefore in the following studies $\mathcal{P} = 4$ will be adopted.

Table 1. Convergence of the energy growth G.

$\mathcal{P}$	G	relative Difference (%)
2	2.0900×10^2	0.50
3	2.0748×10^2	0.20
4	2.0797×10^2	0.02
5	2.0792×10^2	0.00
6	2.0792×10^2	–

IV. Base flow

The unperturbed development of the vortex/ground interaction can be obtained by 2D DNS, as illustrated in figure 2. The contour levels are -0.3 -0.2, -0.1, 0.3, 0.5 and 0.7, with positive and negative levels represented by solid and dashed lines, respectively; the parameters adopted in this base flow calculation are $Re = 1000$, $q = 0.8$, $R = 0.1$ and $T = 50$. These specifications will be used in all the following studies if not otherwise stated. The defaulted value of the swirl strength $q = 0.8$ is aligned with previous studies of an isolated Batchelor vortex.[20,21] The defaulted vortex size, measured by the core radius R, ensures that the vortex

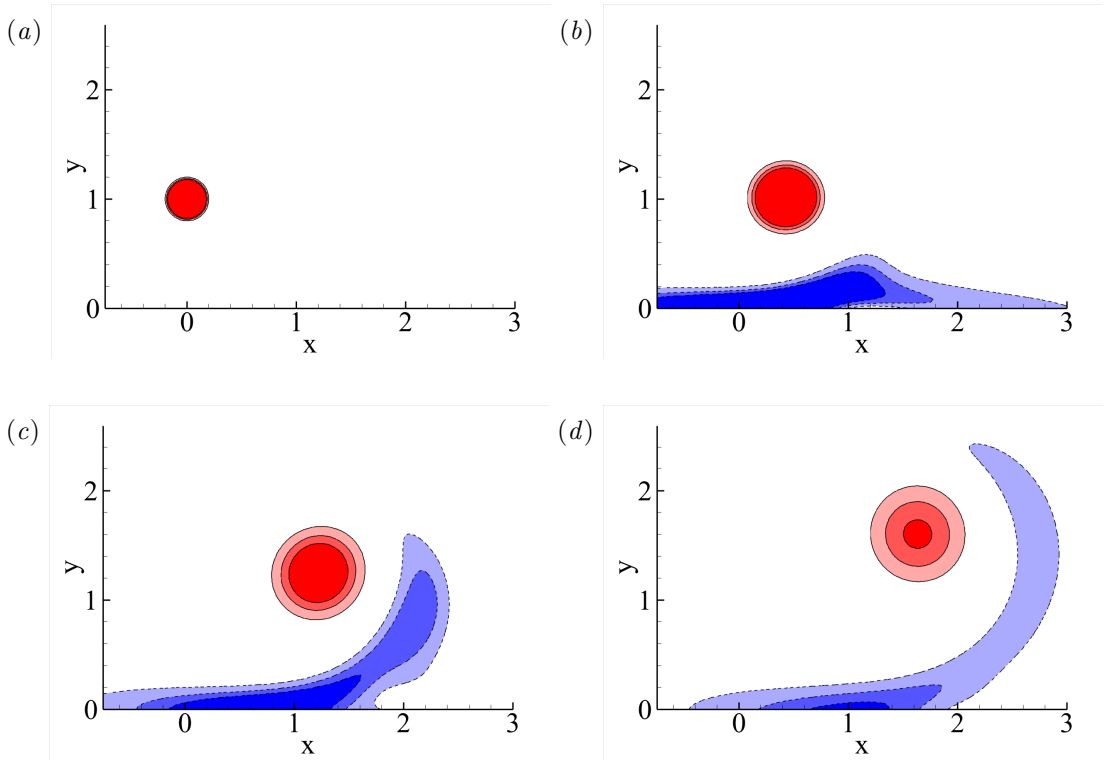

Figure 2. Vorticity contours of the base flow at (*a*) $t = 0$, (*b*) $t = 10$, (*c*) $t = 30$, (*d*) $t = 50$.

and the ground are not decoupled, and that the vortex is not initially distorted by the ground boundary, as can be seen in figure 2(a). It is worth noting that a mirror vortex can be added on the other side of the ground to cancel the initial vertical velocity around the ground. However, a previous investigation suggests that this mirror vortex has only minor influence on the vortex instability.[4]

As the vortex develops, it induces a boundary layer flow with opposite vorticity near the ground. The induced velocity of this boundary vorticity drives the vortex to move in the positive x direction, as observed in figure 2(b). As the flow continues developing, the boundary layer separates and wraps up to form a secondary vortex[1] owing to the flow induced by the main vortex (see figure 2(c)). Then the boundary layer above the ground and the secondary vortex beside the main vortex induce outward (positive x) and upward (positive y) motions, respectively, on the main vortex (see figure 2(d)). This upward motion has been well documented as the "rebound motion".[14] It is also noticed that during the development, the main vortex decays owing to viscous diffusion.

V. Linear transient growth of perturbations

Optimal transient energy growth over a range of streamwise wavenumbers is calculated by integrating the linearised NS equations and the adjoint, and applying an Arnoldi method as discussed in § II. The

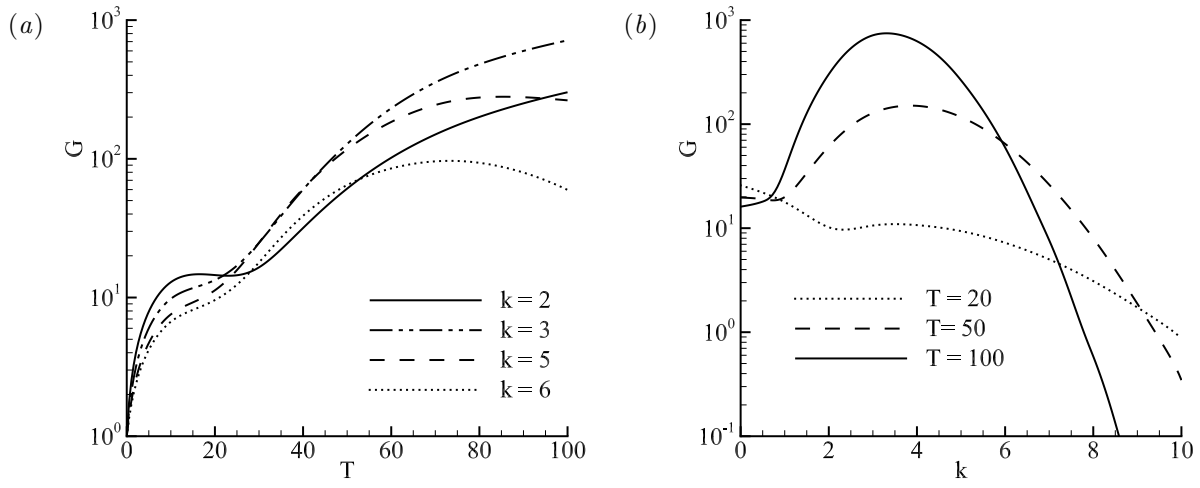

Figure 3. Transient growth as a function of the final time T and streamwise wavenumber k.

transient growth of the perturbations to the base flow shown in figure 2, measured by the maximum gain G, is illustrated in figure 3. It is seen that as the final time T increases, the perturbation growth becomes larger for the $k = 2$ and $k = 3$ cases, indicating that the vortex can be unstable at these cases. For the perturbations with higher wavenumbers, the streamwise distribution becomes more oscillatory and tends to decay due to viscous diffusion. Over the range of streamwise wavenumbers considered, the energy growth reaches 10^3 and maximises at $k = 3.8$.

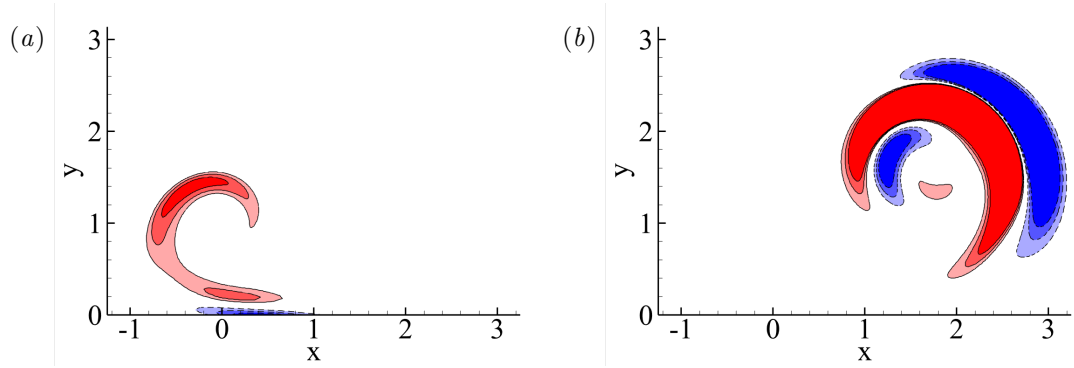

Figure 4. Vorticity contours for (a) the optimal perturbation ($t = 0$) and (b) the corresponding outcome ($t = T = 50$) at $k = 3.8$.

The distribution of the optimal initial perturbation ($t = 0$) and its outcome ($t = T = 50$) at $k = 3.8$ are presented in figure 4. The contour levels are chosen to highlight the structures and are the same in the two plots. It is observed that the initial perturbation is located on one side of the main vortex (downstream of the aileron), and is convected by the base flow to the other side, with the magnitude significantly amplified. The structure of the final outcome is clearly associated with the secondary vortex, indicating that the secondary

vortex is more susceptible to be perturbed by environmental noise. Over small values of T, e.g. $T = 20$, the perturbations are convected to the boundary layer on the ground but do not reach the other side of the main vortex. Therefore the transient growth is associated with the boundary layer flow and maximises at $k = 0$, similarly to the Tollmien-Schlichting waves, as illustrated in figure 3(b). Since the outcome flow consists of a pair of positive/negative vorticity strips and varies sinusoidally in the streamwise direction, it can be expected that the (streamwise averaged) secondary vortex can be suppressed by perturbations, as will be verified in the next section.

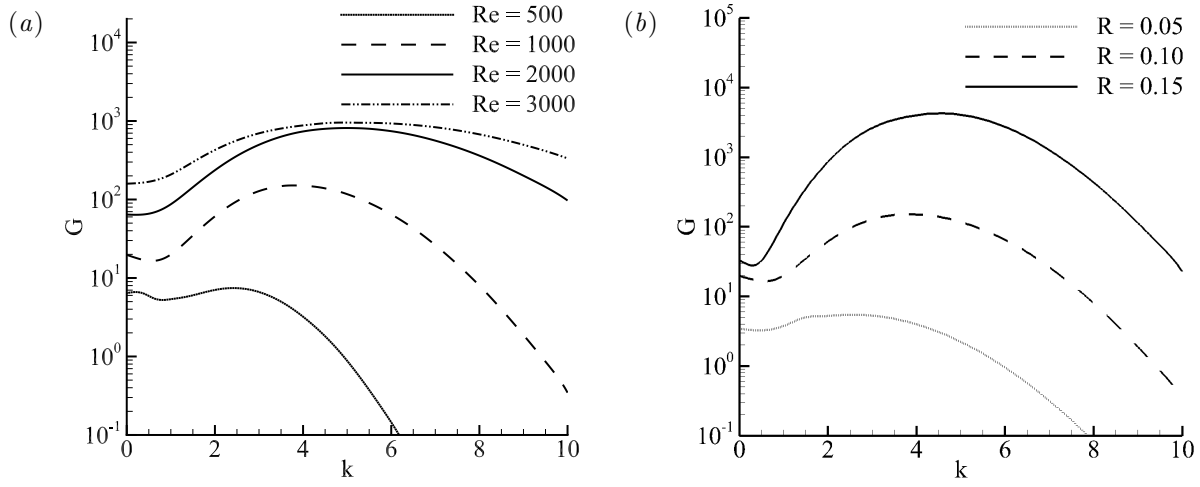

Figure 5. Dependence of the transient growth G on (a) the Reynolds number Re and (b) the vortex core R at $T = 50$.

At higher Re, the boundary layer becomes thinner, so does the secondary vortex. Such a thinner vortex sheet can be more susceptible to perturbations and would undergo stronger transient growth. In figure 5(a), it is seen that as Re increases, the optimal value of k increases and a higher maximum growth is reached. These observations suggest that the transient growth mechanism could be inviscid, in contrast to the viscous rebound effect seen in the base flow development. Transient growth at $Re > 3000$ is conducted (not shown here), and the optimal perturbation is found to be concentrated inside the vortex core and associated with the helical instability of the Batchelor vortex, indicating that the vortex and the ground are decoupled. In this condition, to activate the vortex/ground interaction, a shorter vortex/ground distance is required.

Effects of the vortex size on transient growth are illustrated in figure 5(b). At higher R, the vortex expands and the vortex/ground interaction is strengthened. Subsequently, the optimal value of k increases and the energy growth becomes larger.

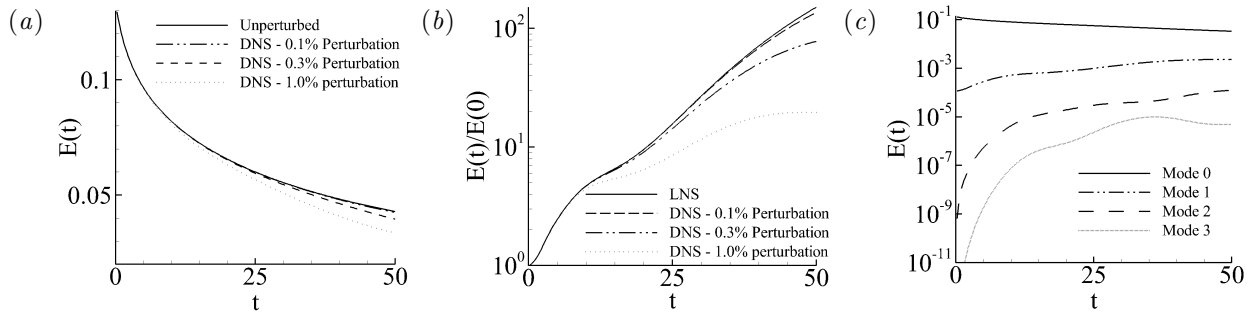

Figure 6. Energy of the optimally perturbed base flow at various perturbation levels obtained in 3D DNS: (a) the base mode; (b) the dominant mode; (c) various modes at perturbation level 1%.

VI. Non-linear evolution of optimal perturbations

The transient energy growth presented above is based on the linear assumption, i.e. the perturbation magnitude is sufficiently small. In this section, perturbations with a finite magnitude will be adopted to perturb the base flow in DNS so as to identify effects of transient growth on the base flow and the nonlinear saturation of the perturbations. In the streamwise direction, a periodic boundary condition is adopted and the streamwise domain length is set to $2\pi/3.8$, so as to accommodate the linearly most energetic perturbation presented in figure 4(a). Sixteen Fourier modes, with streamwise wavenumber 0, $2\pi/3.8$, $4\pi/3.8$, ..., $30\pi/3.8$, are calculated. The first, second, and following modes will be denoted as the base mode, dominant mode and higher harmonics, respectively. Perturbations with magnitude levels 0.1%, 0.3% and 1% (square root of the ratio of initial perturbation energy and base flow energy) are tested. From figure 6(a), it is seen that the development of perturbations induces decay of the energy of the base mode. As will be discussed later, this energy decay is associated with the suppression of secondary vortices. In figure 6(b), it can be observed that the energy growth of the dominant mode in nonlinear developments (normalized by the initial energy) almost overlaps with the linear prediction (denoted by "LNS") at small enough perturbation levels, while deviates from the latter as the initial perturbation becomes larger (). The nonlinear saturation of the dominant mode and the higher harmonics can be clearly observed in figure 6(c).

In the following studies, the perturbation energy level will be fixed at 1%. The perturbed flow is averaged in the streamwise direction, as shown in figure 7. Comparing against the unperturbed flow in figure 2, the separation and wrap-up of the boundary layer, the generation of the secondary vortex, and subsequently the rebound motion, are significantly suppressed by perturbations. Effects of perturbations on both the secondary and main vortices can be clearer seen in figure 8. It is noticed that at higher levels of perturbations, the main vortex is less rebounded, and the boundary layer separation and the secondary vortex become weaker.

After presenting the streamwise averaged flow, the 3D flow patterns are illustrated in figure 9. All

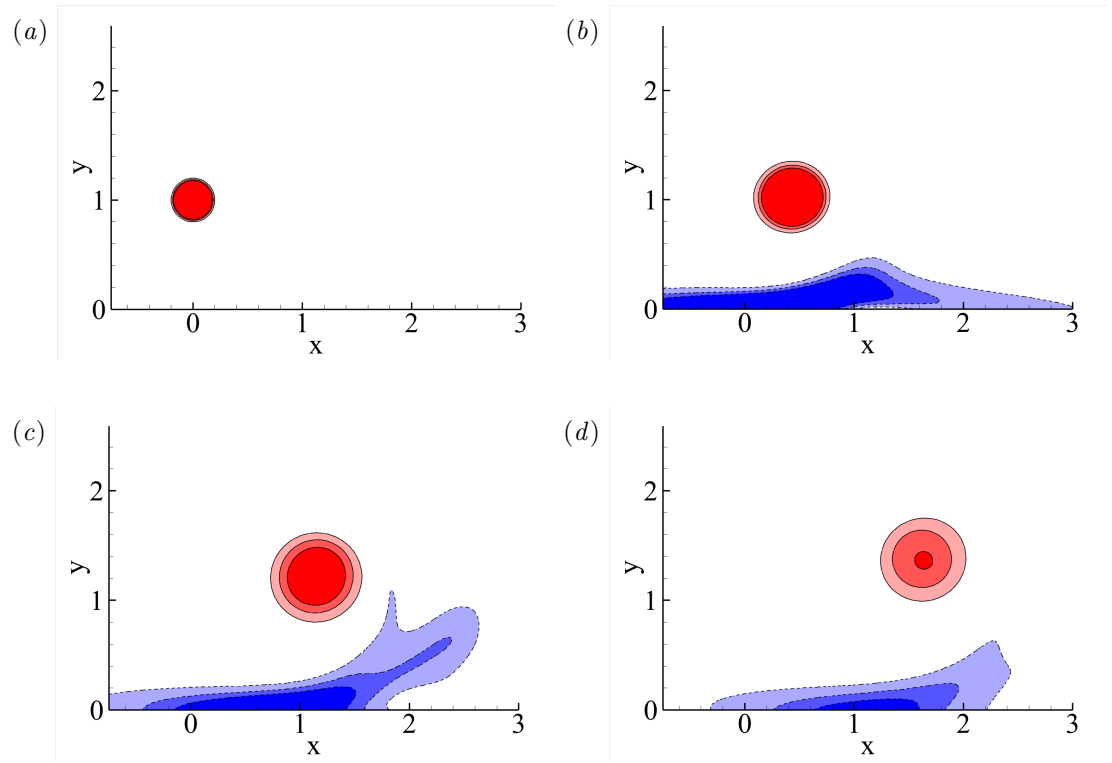

Figure 7. Vorticity contours of the optimally perturbed flow with perturbation level 1% at (*a*) $t = 0$, (*b*) $t = 10$, (*c*) $t = 30$ and (*d*) $t = 50$.

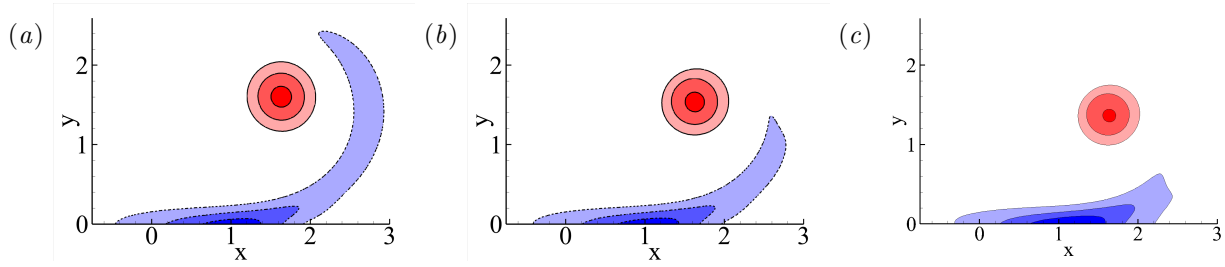

Figure 8. Vorticity contours of the optimally perturbed flow at $t = 50$ with initial perturbation level (*a*) 0, (*b*) 0.3%, and (*c*) 1%.

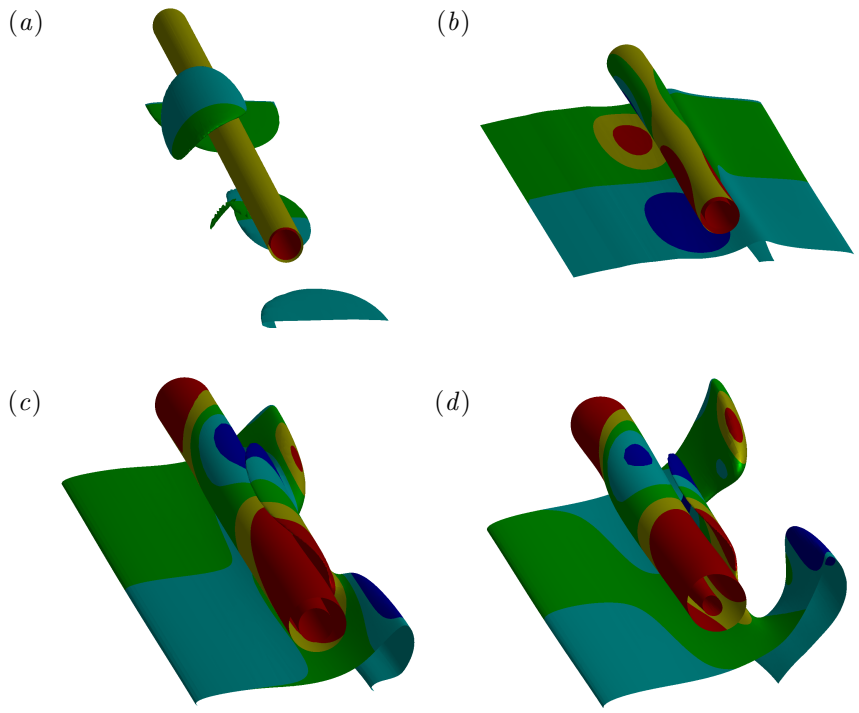

Figure 9. Iso-surfaces of streamwise vorticity, coloured by streamwise velocity, at (*a*) $t = 0$, (*b*) $t = 10$, (*c*) $t = 30$ and (*d*) $t = 50$. The flow is initially perturbed by the optimal perturbation with level 1%.

the parameters are the same as used in figure 7. It is seen that the secondary vortex is in a sinusoidal form, indicating that this vortex sheet is dominated by perturbations. Since the streamwise average of the perturbation is zero, the mean secondary vortex is suppressed, as has been observed in figure 7. The wavy form of the main flow can also be noticed, owing to the variation of the induced velocity generated by the secondary vortex.

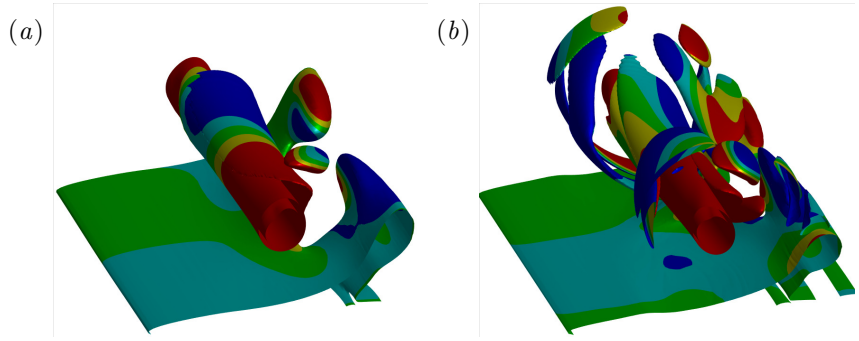

Figure 10. Iso-surfaces of streamwise vorticity, coloured by streamwise velocity, at $t = 50$ and (*a*) $Re = 2000$ and (*b*) $Re = 3000$. The flow is initially perturbed by the optimal perturbation with level 1%.

It can be expected that at higher Reynolds number, the large coherent structures shown in figure 9 break down to turbulence. The developments of optimally perturbed flow at $Re = 2000$ and 3000 are studied in

DNS using 32 spanwise Fourier modes, as illustrated in figure 10. The thin shear layer associated with the secondary vortex is broken to small eddies around the periphery of the main vortex. DNS at $Re > 3000$ are also conducted but not presented here, since the perturbation dynamics are associated with the helical instability of the Batchelor vortex, instead of the vortex/ground interaction. As discussed above, in these higher Reynolds number conditions, a vortex closer to the ground or a larger value of R is required to study the vortex/ground interaction.

VII. Conclusions

A simplified model is established to investigate the effects of perturbations on vortex/ground interactions. The vortex is modelled as the Batchelor vortex, and a typical swirl strength $q = 0.8$ well explored in literature[20,21] is used throughout this work. The boundary layer separation, secondary vortex generation and rebound motion of the main vortex are all observed in 2D DNS of the unperturbed flow.

Using the unperturbed flow as base flow, the optimal initial perturbations at various streamwise wavenumbers and final times can be calculated using a well-established Arnoldi method. Over the parameters studied, the most energetic perturbation appears at streamwise wavenumber $3 \sim 5$. The maximum energy growth increases at higher Reynolds number or larger vortex sizes, at which the vortex/ground interaction is strengthened, suggesting that the transient growth is associated with this interaction, rather than the dynamics of the isolated main vortex. The most energetic initial perturbation is located on one side of the main vortex and can be considered as a component of the free-stream turbulence or wake flow downstream of the ailerons. During the development, this initial perturbation is convected towards the ground and then wrapped up to interact with the secondary vortex.

In nonlinear evolution of the optimal perturbation, the perturbation suppresses the secondary vortex and subsequently weakens the rebound motion. The 3D variation of the perturbed flow indicates that the main vortex core is distorted and the secondary vortex is dominated by perturbations. This study suggests that the widely reported strong rebound in 2D simulations would be significantly weakened in real 3D studies owing to transient effects associated with external noise.[11,14] The nonlinear transient effects also contribute to explain the widely observed 3D variation and asymmetry of the secondary vortices.[3,4,6,10]

References

[1]Harvey, J. K. and Perry, F. J., "Flowfield produced by trailing vortices in the vicinity of the ground," *AIAA J.*, Vol. 9, 1971, pp. 1659–1660.

[2]Lamb, H., *Hydrodynamics - 6th Edition*, Cambridge University Press, 1932.

[3]Stephan, A., Holzäpfel, F., and Misaka, T., "Hybrid simulation of wake-vortex evolution during landing on flat terrain and with plate line," *Int. J. Heat Fluid Flow*, Vol. 49, 2014, pp. 18–27.

[4]Harris, D. M. and Williamson, C. H. K., "Instability of secondary vortices generated by a vortex pair in ground effect," *J. Fluid Mech.*, Vol. 700, 2012, pp. 148–186.

[5]Wetmore, J. W. and Reeder, J. P., "Aircraft Vortex Wakes in relation to Terminal Operations," Tech. Rep. D-1777, NASA, 1963.

[6]Holzäpfel, F. and Steen, M., "Aircraft WakeVortex Evolution in Ground Proximity: Analysis and Parameterization," *AIAA J.*, Vol. 45, 2007, pp. 218–227.

[7]Stephan, A., Holzäpfel, F., and Misaka, T., "Aircraft Wake-Vortex Decay in Ground ProximityPhysical Mechanisms and Artificial Enhancement," *J. Aircraft*, Vol. 50, 2013, pp. 1250–1260.

[8]X. Zhang, A. S. and Ruhrmann, A., "Vortices behind a bluff body with an upswept aft section in ground effect," *International Journal of Heat and Fluid Flow*, Vol. 25, 2004, pp. 1–9.

[9]Katz, J., "Aerodynamics of Race Cars," *Annu. Rev. Fluid Mech.*, Vol. 38, 2006, pp. 27–63.

[10]Lawson, N., Knowles, K., Bray, D., Finnis, M., and Eyles, J., "Transient and time-averaged characteristics of a compressible ground vortex flow," *J. Aerospace Engineering*, Vol. 228, 2014, pp. 375–383.

[11]Eriksson, S., Svärd, M., and Nordström, J., "Simulations of ground effects on wake vortices at runways," Tech. rep., Center for Turbulence Research, Annual Research Briefs, 2007.

[12]Murphy, D. and Mao, X., "Suppresion of Vorticity in Vortex and Pipe Flow Interactions," *Theoretical and Computational Fluid Dynamics*, Vol. 29, 2015, pp. 55–65.

[13]Spalart, P. R., Strelets, M. K., Travin, A. K., and Shur, M. L., "Modeling the Interaction of a Vortex Pair with the Ground," *Fluid Dynamics*, Vol. 36, 2001, pp. 899–908.

[14]Victor, X. S. and Puel, F., "Interaction of wake vortices with the ground," *Aerosp. Sci. Technol.*, Vol. 4, 2000, pp. 239–247.

[15]Schmid, P. J., "Nonmodal Stability Theory," *Annu. Rev. Fluid Mech.*, Vol. 39, 2007, pp. 129–162.

[16]Barkley, D., Blackburn, H. M., and Sherwin, S. J., "Direct Optimal Growth Analysis for Timesteppers," *Int. J. Num. Meth. Fluids*, Vol. 57, 2008, pp. 1435–1458.

[17]Fabre, D., Jacquin, L., and Loof, A., "Optimal perturbations in a four-vortex aircraft wake in counter-rotating configuration," *JFM*, Vol. 451, 2002, pp. 319–328.

[18]Mao, X., Sherwin, S. J., and Blackburn, H. M., "Non-normal dynamics of co-rotating vortex pairs," *J. Fluid Mech.*, Vol. 701, 2012, pp. 430–459.

[19]Karniadakis, G. E. and Sherwin, S. J., *Spectral/hp Element Methods for Computational Fluid Dynamics*, Oxford University Press, 2nd ed., 2005.

[20]Broadhurst, M. S. and Sherwin, S. J., "Helical Instability and Breakdown of a Batchelor Trailing Vortex," *Mathematics in Industry*, Vol. 12, 2008, pp. 191–195.

[21]Mao, X., Blackburn, H. M., and Sherwin, S. J., "Calculation of global optimal initial and boundary perturbations for the linearised incompressible Navier–Stokes equations," *J. Comput. Phys.*, Vol. 235, 2013, pp. 258–273.